Rev. Adv. Mater. Sci. 33 (2013) 195-201

NUMERICAL STUDY ON BUBBLE RISING BEHAVIOR IN A RECIPROCALLY STIRRED MOLTEN METAL FLOW

Hong Liu[1], Mao-Zhao Xie[1], Hong-Sheng Liu[1] and De-Qing Wang[2]

[1]School of Energy and Power, Dalian University of Technology, Dalian, 116024, China
[2]School of Materials Science and Engineering, Dalian jiaotong University, Dalian, 116024, China

Received: October 17, 2011

Abstract. A feasible approach to obtain the bubble diameter homogeneity is using an air injector moving in reciprocating shift instead of the pitched-blade impeller used previously. This paper reports progress in the numerical simulations of movement and deformation of a single bubble in a reciprocally stirred liquid metal flow field. The volume-of fluid (VOF) method was used for tracking the interface between the bubble and the melt flow. A dynamic mesh method was used to predict the bubble-melt flow in a two-dimensional foaming tank. The influences of reciprocating frequency and bubble diameter on the behavior of bubble movement and deformation in the melt flow were discussed. Results show that the bubble movement trajectory and the behavior of bubble deformation is dependent on bubble diameter and reciprocating frequency, the oscillations in the bubble trajectory become more intensive with increasing bubble diameter and decreasing reciprocating frequency.

1. INTRODUCTION

Aluminum foams are a kind of very useful and promising functional materials. The advancement in the techniques for production of aluminum foams has expanded their use over a wide range of applications [1,2]. Among many approaches for the production of aluminum foams, the gas injection method has outstanding advantages in the respect that foams can be produced continuously and the size of the product is little limited [3]. In this technique, air is injected through a nozzle into molten aluminum composites, forming a liquid foam body, which is stabilized by the presence of solid ceramic particles at gas-liquid interfaces of the cell walls. The stabilized liquid foam is then mechanically conveyed off the surface of the melt and allowed to cool to form a solid slab of aluminum foam.

Foam properties depend widely on the gas content, the air bubble size and size distribution as well as on the bubble movement and deformation behavior. A large number of works have been published concerning bubble formation and rising behavior, *e.g.*, liquid circulation in bubble columns [4], bubble formation at a submerged orifice in the quiescent liquid [5], or rising behavior of single air bubbles in liquid cross-flow [6-9].

The key question in the foaming production is ensuring a homogeneity of bubble size and of its distribution in the molten metal flow field. As indicated by our experiment [10], a feasible approach to obtain the bubble diameter homogeneity is using an air injector moving in a reciprocating shift instead of the pitched-blade impeller used previously. The presence of a liquid cross-flow induced by the reciprocating shift offers two major advantages: first, smaller bubbles are produced when compared to bubble formation under quiescent liquid conditions; second, the detached bubbles tend to be swept away from the region around the orifice, thereby reducing the likelihood of bubble coalescence. However, the

Corresponding author: Hong Liu, e-mail: hongliu@dlut.edu.cn

role of reciprocating cross-flow on bubble movement behavior has not been systematically studied.

The objective of this study is to numerically investigate characteristics of the bubble movement behavior in a reciprocally stirred molten metal flow and to clarify the effects of working parameters, *e.g.* the reciprocating frequency and the bubble diameter on the bubble deformation and bubble movement trajectory, and on this basis, to gain an insight into their effects on the foam structure.

2. NUMERICAL APPROACH

The flow induced by an air injector moving in the reciprocating shift is considered here as two-dimension, incompressible and laminar. For both the liquid flow outside the bubble and the gas flow inside the bubble, the governing equations can be written as follows based on the Navier-Stokes equations with extra terms which take into account the forces due to the surface tension and gravity. The continuity equation:

$$\frac{\partial \rho}{\partial t} + \nabla \cdot (\rho U) = 0. \tag{1}$$

The momentum equation:

$$\frac{\partial (\rho U)}{\partial t} + \nabla \cdot (\rho U) = -\nabla p + \nabla \cdot \left[\mu \left[\nabla U + \nabla U^T \right] \right] + \rho g + F_{bf}, \tag{2}$$

where U denotes the velocity vector; t is the time; p, g, denote the pressure and the gravitational acceleration, respectively, and F_{bf} is the interface force per unit volume and will be given in section 2.2.

2.1. VOF method

For identifying each phase in the two-phase flow separately, a volume fraction, denoted by C, is introduced following the volume of fluid method (VOF) proposed by Hirt and Nichols [11] and improved by many scholars [12,13]. The movement of the gas-liquid interface is tracked based on the distributions of $C(x,t)$, the volume fraction of gas in a computational cell, where $C(x,t) = 1$ in the gas phase and $C(x,t) = 0$ in the liquid phase. Therefore, a gas-liquid interface exists in the cells where $C(x,t)$ lies between 0 and 1. The piecewise linear interface calculation (PLIC) method is applied to reconstruct the bubble free surfaces with a multidimensional algorithm to determine the slope of the interface in each reconstructed cell.

The advection equation for $C(x,t)$ is given by

$$\frac{\partial C}{\partial t} + (U \cdot \nabla) C = 0. \tag{3}$$

The value of density and viscosity are calculated as functions of C, using linear interpolation between the values of the two phases:

$$\begin{aligned} \rho &= \rho_g C + \rho_l (1 - C), \\ \mu &= \mu_g C + \mu_l (1 - C). \end{aligned} \tag{4}$$

2.2. Model for interfacial forces

The effect of the surface tension force is incorporated in the computation of the velocity and pressure fields via an equivalent surface pressure. The value of interfacial force F is equal to

$$\mathbf{F} = \sigma \frac{\rho \kappa \nabla C}{1/2 (\rho_l + \rho_g)},$$

where σ is the numerical value of the surface tension and κ is the curvature of the interface.

The curvature of the interface may be expressed in terms of the divergence of the unit normal vector to the interface, as follows:

$$\kappa = \nabla \cdot (\nabla C / |\nabla C|). \tag{5}$$

2.3. Model for the injector reciprocating shift

In the present study, numerical simulations on single bubble dynamics in a reciprocating liquid metal flow are conducted, however, the bubble formation process is not taken into account at this stage. A moving mesh method is used to describe the reciprocating cross flow. The transverse velocity of the air injector in the horizontal direction can be deduced from the reciprocating movement as follows:

$$u = R\omega \cos \alpha, \tag{6}$$

where R is the crank radius (mm), ω is crank shaft speed (rad/s), α is crank rotational angle (rad). In this study R = 14 mm. The schematic diagram of reciprocating configuration is shown in Fig. 1.

2.4. Boundary and initial conditions

All simulations reported here were carried out in a rectangular vessel of 130 mm in length and 250 mm in height with 3 no slip walls and an exit at the top.

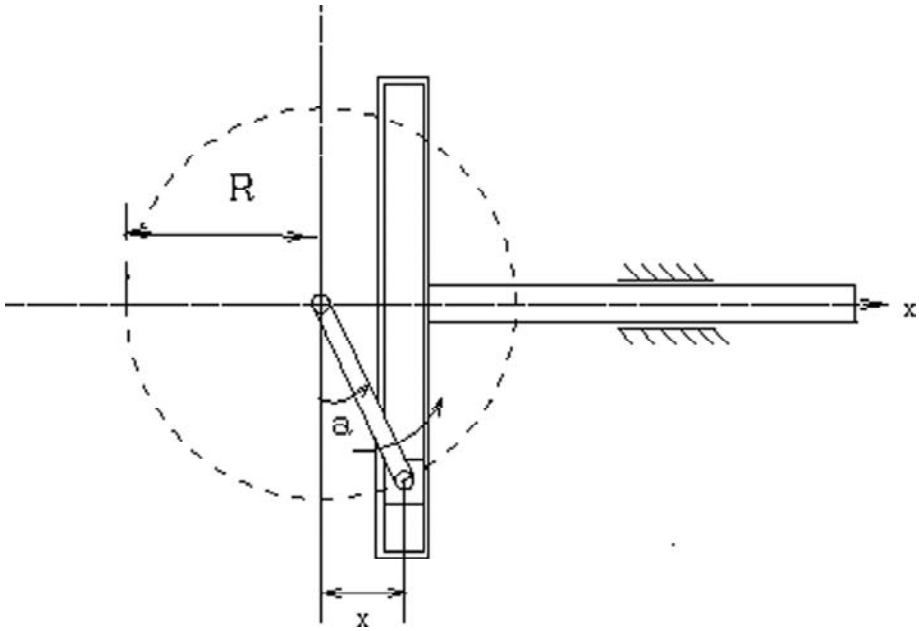

Fig. 1. Schematic diagram of reciprocating configuration.

The vessel is initially filled with liquid aluminum. The vessel is modeled as an open system, so the pressure in the space above the initial liquid top surface is equal to the ambient pressure (1.01325×10^5 Pa). A reciprocating moving block (representing the injector) is set in the liquid aluminum with its top surface being at the level of 25 mm from the vessel bottom. At the block walls the no slip and impermeability conditions are applied. The frequencies of the reciprocating movement of the block used in the calculations are 50, 100, and 200 RPM. The initial location of the center of the spherical gas bubble is specified at 35 mm above the bottom center of the computational domain. Three bubble sizes of 4, 6, 8 mm in diameter are studied. Gas and liquid properties are set as follows: density of aluminum melt: ρ_l = 2600 kg/m^3, and viscosity μ_l = 0.00375 Pa s; air density ρ_g = 1.225 kg/m^{3}and viscosity $\mu_g = 1.79\times10^{-5}$ Pa s

For simplicity, the formation of fluctuations on the top liquid surface was neglected so that the surface remains flat throughout the computation. In addition, no liquid is allowed to pass through the top boundary.

2.5. Solution procedure

The governing partial differential equations are discretized by the finite volume method. The discretisation of the convection terms is based on a second-order, upwind method, whilst the volumetric fraction equations are solved with the QUICK scheme. The PISO algorithm is used for the pressure-velocity coupling and the PRESTO scheme for pressure discretization. The time derivative was discretized using a second-order differencing scheme. Converged solution is considered to be reached when the residuals of all the variables are smaller than 10^{-5}.

A non-uniform 2D Cartesian co-ordinate grid is employed. To determine the optimum mesh size, a mesh independence study has been performed with three non-uniform grid sizes which have 320×500, 280×435, 240×350 control volumes respectively, correspondently, 80, 100, and 120 elements are positioned in the initial bubble. It was found that computational results changed little when mesh cells increased from 280×435 to 320×500. To keep a lower computation cost, all simulations of this work were carried out with the grid of 280×435. For the time dependent VOF calculations of the Eq. 3, explicit time-marching scheme with a very small Courant number of

$$C_0 = \frac{u_d \Delta t}{\Delta x} < 0.2$$

for all grid sizes was used. So the time step used in the simulations was usually 10^{-5} sec or even smaller.

3. RESULTS AND DISCUSSION

Simulation results were first examined and compared with the data of Li'experiments [8] in order to bench mark our computational methods. The simulation results of the rise velocity are in good agree-

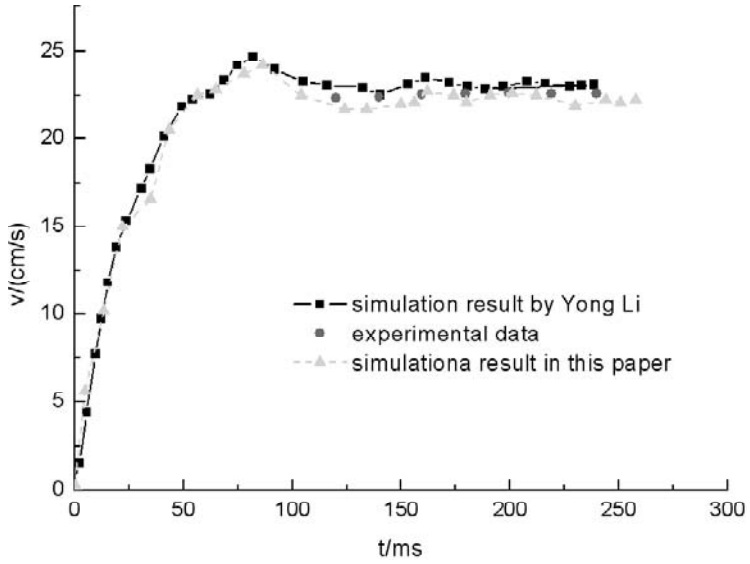

Fig. 2. Bubble rising velocity: comparison of simulation and experimental data.

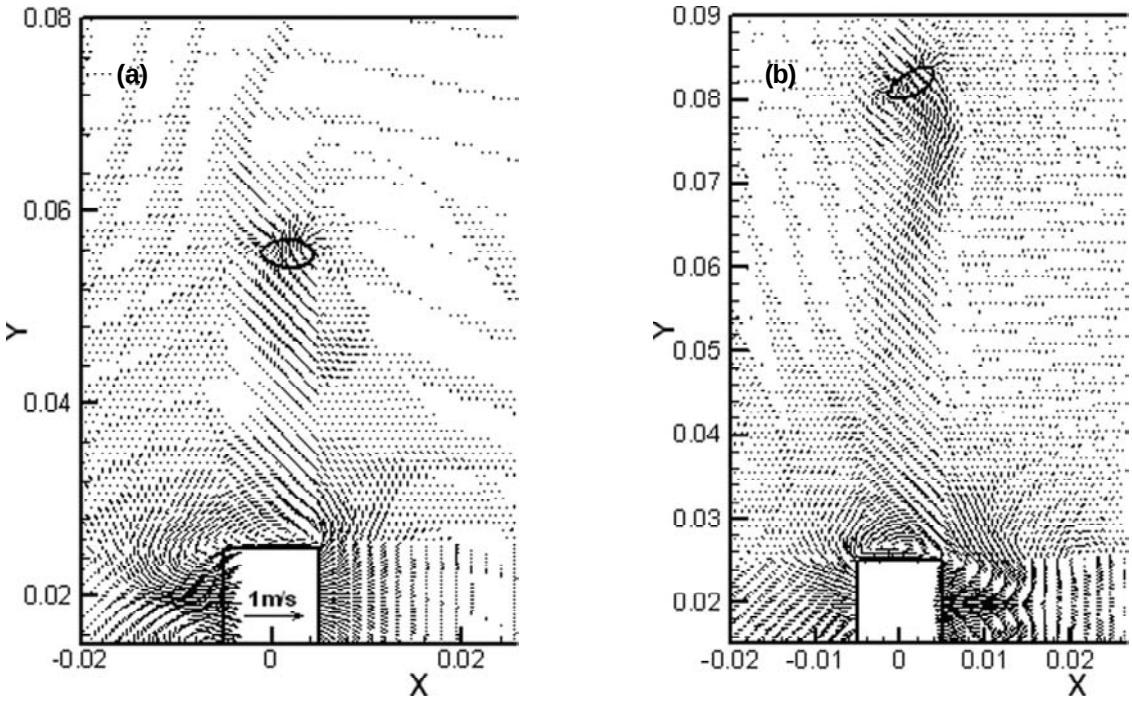

Fig. 3. Instantaneous bubble shapes and velocity vector. (a) t = 150 ms; (b) t = 300 ms.

ment with the experimental data, as shown in Fig. 2. It can be seen that the present model reasonably captures the flow behavior of the gas phase.

The characteristics of a rising bubble in the reciprocating stirred melt flow can be described in terms of the shape, rise velocity, and motion trajectory of the bubble, as discussed in the following.

3.1. Bubble shape

The instantaneous bubble shape of an initially spherical gas bubble with d_b = 4 mm and the flow velocity vector distribution around it at two different time are shown in Fig. 3. It is noted that there exists a circulation zone on the top of block due to the reciprocating movement of the block. At beginning the bubble movement is affected obviously by the reciprocating movement of the block, so its velocity direction is reverse with the direction of the block shift, which is due to the circulation. Meanwhile two asymmetric vortices can be observed closely behind the rising bubble due to the bubble rise velocity. The higher the bubble ascends up, the weaker the effects of the block shift movement on the bubble become.

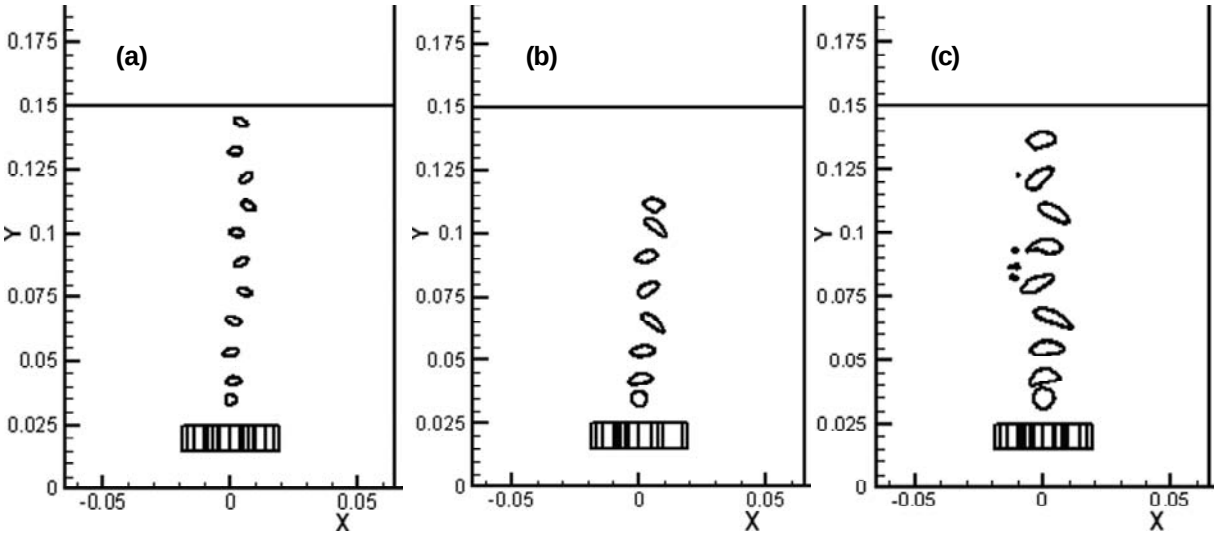

Fig. 4. Effects of bubble diameter on bubble rise trajectories. (ω = 100 rpm, Δt = 66.67 ms), (a) d_b = 4 mm; (b) d_b = 6 mm; (c) d_b = 8 mm.

The simulated snapshots of instantaneous bubble shapes and trajectories of air rising in the molten aluminum are shown in Fig. 4, where three cases are presented for a constant shift frequency (ω = 100 rpm) and different bubble diameters. The time interval between any two adjacent bubbles is 66.67 ms.

The trajectory of small air bubble (d_b = 4 mm and d_b = 6 mm) is found to be steadily migrating towards the liquid top surface. The bubble shape changes from the initial imposed spherical to ellipsoidal. As the bubble size is increased to d_b = 8 mm, the trajectory of the bubble is found migrate very similar to the case of d_b = 4 mm, while a significant bubble deformation is observed and the lower part of the bubble becomes thinner and thinner and eventually the bubble seems a distorted oblate spheroid, a small part could be splited from the rim of the bubble and breakup. The breakup of the bubble is visible for the bubble with d_b = 8 mm after 330 ms, whilst a breakup does not happen for the smaller bubbles.

Snapshots of typical bubble trajectories influenced by the frequency of the reciprocating shift are shown in Fig. 5. In the case of r = 2 mm, ω = 0 rpm (*i.e.* quiescent liquid), bubble shape changes from spherical to ellipsoidal in a wobbling regime, the bubble moves outward due to the action of the lateral lift, and the oscillations in the bubble trajectory is significant. For the case of ω = 100 rpm, a small oscillations can be seen in the bubble trajectory, the bubble rises in a zigzag path. For the case of ω = 200 rpm, bubble moves upwards in a nearly symmetric path. This means that its amplitude decreases with increasing the frequency. The reason for this phenomenon might be that the lift, which induced by the co-action of the upward motion of the bubble and the circulation around its cross section, is suppressed by the reciprocating shift of the block at higher frequencies.

3.2. Bubble velocity

The predicted values of bubble rise velocities and transverse velocity for three different bubble diameters are plotted as a function of time as shown in Fig. 6. It can be seen clearly that the rise component of bubble velocities is much larger than the transverse component at the initial stage. With increasing time, the transverse velocity is gradually enlarged to the same order of magnitude as the upward velocity. Both the rise and transverse velocities undergo augmenting fluctuations during the rising process. The wobbling behavior of the bubble is found to increase with increasing in the bubble diameter.

The effects of reciprocating frequency on bubble movement behavior are shown in Fig. 7. In the quiescent flow, the oscillations of the bubble terminal rising velocity are significant. Importantly, it should be noted that with increase in the frequency of shift, both the rise and transverse velocities tend to be stable with less fluctuations.

4. CONCLUSION

Numerical simulations were conducted to explore the bubble deformation and movement behavior in

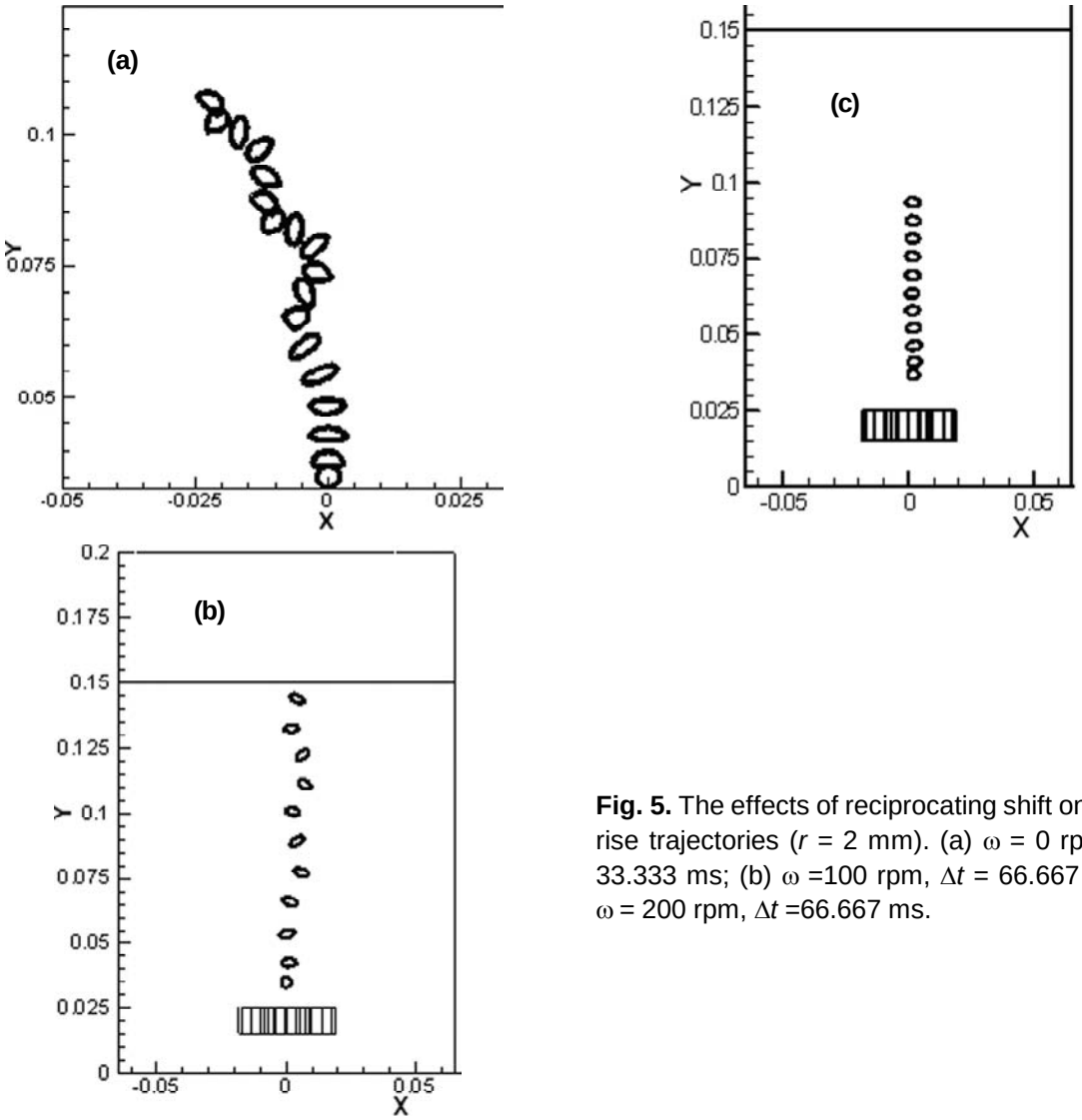

Fig. 5. The effects of reciprocating shift on bubble rise trajectories (r = 2 mm). (a) ω = 0 rpm, Δt = 33.333 ms; (b) ω =100 rpm, Δt = 66.667 ms; (c) ω = 200 rpm, Δt =66.667 ms.

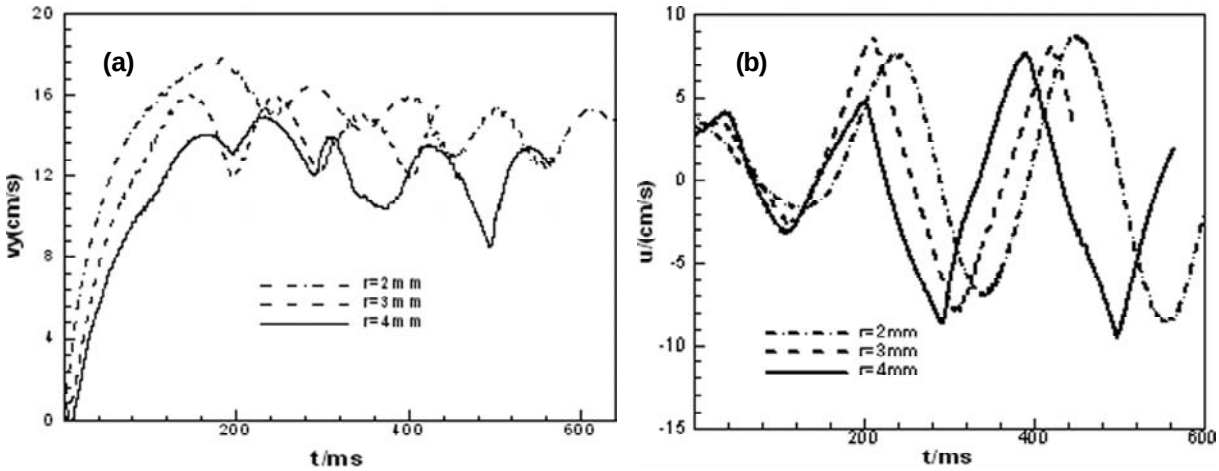

Fig. 6. The effects of bubble diameter on bubble velocity. (a) rise velocity; (b) transverse velocity.

the reciprocating stirred liquid metal flow. The simulations were carried out using the volume of fluid technique incorporating with a dynamic mesh method. The effects of bubble diameter and stroke velocity on the bubble velocity and trajectory were studied. Results show that a larger bubble suffers breakup more frequently in comparison with smaller one, and that the bubble movement trajectory is

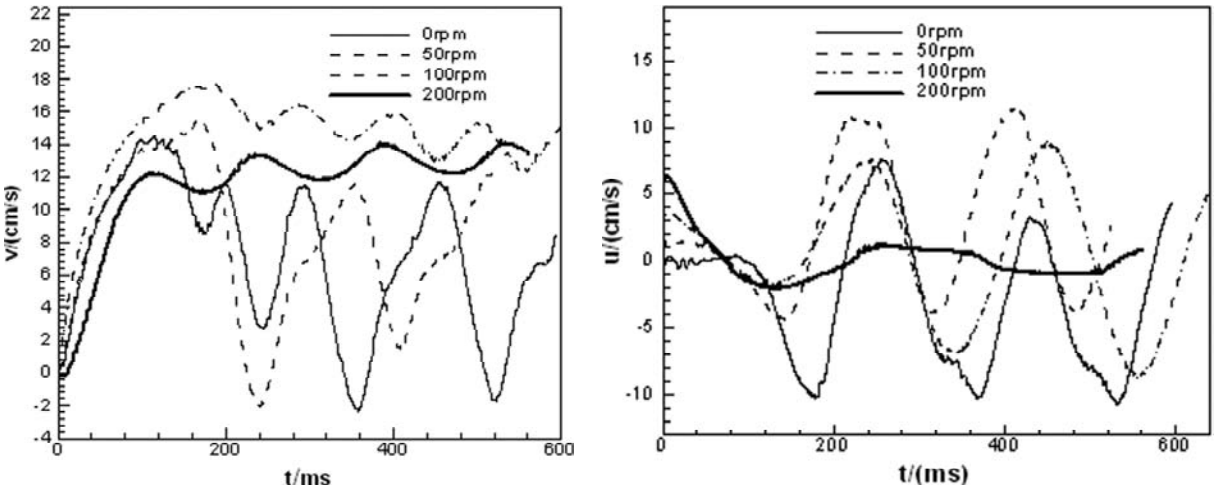

Fig. 7. The effects of reciprocated frequency on bubble velocity. (a) rise velocity; (b) transverse velocity.

dependent on bubble diameter and reciprocating frequency, the oscillations in the bubble trajectory become more intensive with increasing bubble diameter and decreasing reciprocating frequency.

ACKNOWLEDGEMENTS

The authors would like to acknowledge support to this work by the National Natural Science Foundation of China (NSFC Grant Nos. 50876017, 50876016,51076109).

REFERENCES

[1] D. Schwingel, H.W. Seeliger and C.Vecchionacci // *Acta Astronautica* **61** (2007) 326.

[2] Q.W. Cheng, W. Altenhof, S.Y. Jin, C. Powell and A.M .Harte // *Int J Mech Sci* **48** (2006) 223.

[3] D.Q. Wang and Z.Y. Shi // *Materials Science and Engineering* **361A** (2003) 45.

[4]Y. Alhendal, A.Turan and Wael I. A. Aly // *Procedia Computer Science* **1** (2010) 673.

[5] D.Gerlach, N.Alleborn, V.Buwa and F.Durst // *Chemical Engineering Science* **62** (2007) 2109.

[6] G.L. Lane, M.P. Schwarz and G.M. Evans // *Applied Mathematical Modeling* **26** (2002) 223.

[7] D. Bothe, M. Schmidtke and H.J. Warnecke // *Chemical Engineering Technology* **29** (2006) 1048.

[8] Y. Li, J.P. Zhang and L.-Sh. Fan // *Chemical Engineering Science* **55** (2000) 4597.

[9] R.Krishna and J.M.Baten // *Int. Comm..Heat Mass Transfer.* **26** (1999) 965.

[10] D.Q. Wang and Ch.X. Sun // *J. Mater. Sci.* **43** (2008) 2825.

[11] C.W. Hirt and B.D. Nichols // *Journal of Computational Physics* **39** (1981) 201.

[12] D. Lorstad and L. Fuchs // *Journal of Computational Physics* **200** (2004) 153.

[13] H Wang, Zh.Y. Zhang, Y.M.Yang and H.Sh.Zhang // *Journal of Hydrodynamics* **22** (2010) 81.